**Supporting Information**

# Synthesis of High Surface Area CaSO$_4$·0.5H$_2$O Nanorods using Calcium Ethoxide as Precursor

Miguel Burgos-Ruiz, Gloria Pelayo-Punzano, Encarnacion Ruiz-Agudo,

Kerstin Elert, and Carlos Rodriguez-Navarro*

Dept. Mineralogy and Petrology, University of Granada, Fuentenueva s/n,

18002 Granada (Spain)

***This document includes:***

**Materials and Methods**

Synthesis of nanobassanite

Characterization of precursor and product phases

Preparation of β-hemihydrate (plaster of Paris) control

Measurement of the hydration kinetics

Cost estimate, potential applications and environmental impact

**Supplementary References**

S1-S8

**Supplementary Figures**

Figure S1. FTIR of precursor calcium ethoxide

Figure S2. XRD pattern of a sample prepared in the absence of toluene

Figure S3. TEM images of a sample prepared in the absence of toluene

Figure S4. TG-DSC analysis of a sample prepared in the absence of toluene
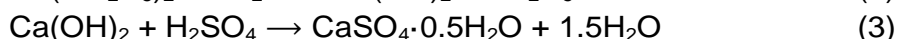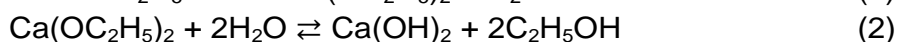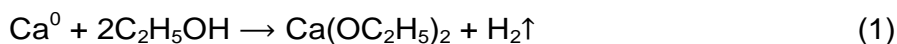
**Supplementary Tables**

Table S1. List of codes and minerals used in XRD analysis

Table S2. Cost estimate of the production of nanobassanite according to the method reported here (excluding labor cost)

## Materials and Methods

### Synthesis of nanobassanite:

Bassanite nanorods were obtained through a solvothermal route involving the formation of amorphous calcium ethoxide and its subsequent reaction with sulfuric acid, as described by the following reactions:

$$Ca^0 + 2C_2H_5OH \rightarrow Ca(OC_2H_5)_2 + H_2\uparrow \qquad (1)$$
$$Ca(OC_2H_5)_2 + 2H_2O \rightleftarrows Ca(OH)_2 + 2C_2H_5OH \qquad (2)$$
$$Ca(OH)_2 + H_2SO_4 \rightarrow CaSO_4 \cdot 0.5H_2O + 1.5H_2O \qquad (3)$$

The overall synthesis consists of three consecutive stages performed in a single reactor (i.e., one pot synthesis). Below we describe these stages for a typical synthesis run:

a) During the first stage (Eq. (1)), the irreversible redox reaction between 2 g of metallic calcium (99 %, granular, Scharlau) and 200 mL of absolute ethanol (Scharlau) occurs for 24 h at 78 °C under reflux condensation, under anhydrous conditions and constant magnetic stirring in a 500 mL glass (or Teflon®) reactor. This step results in a whitish ethanolic suspension of calcium ethoxide, which serves as initial precursor of the bassanite nanoparticles.

b) During the second stage, 80 mL of toluene (99.9 %, Scharlau) and 10 mL of a 5M sulfuric acid solution (prepared from $H_2SO_4$, 95-98 %, Sigma-Aldrich) pre-heated to 78 °C, are added (dropwise) into the suspension previously obtained. The reaction progresses at 78 °C under continuous magnetic stirring for different periods of time: 35, 45, 55 and 60 minutes. This promotes the following simultaneous processes: On the one hand, sulfuric acid can directly react with calcium alkoxide particles in the suspension, while the presence of water enables the hydrolysis of these precursor particles originating $Ca(OH)_2$, an intermediate species that is later neutralized by the sulfuric acid. Both pathways converge in the precipitation of $CaSO_4 \cdot 0.5H_2O$ as the final product.

c) The final stage involves the separation of the bassanite nanoparticles from the mixture of solvents through rotary evaporation at 80 °C and ~7 mbar. The obtained solids are then oven-dried at 80 °C for 30 minutes and stored under $N_2$ atmosphere.

The yield of this typical synthesis run was ≥ 99% (as determined from thermogravimetry analysis results; see below), resulting in the production of ~14 g of $CaSO_4 \cdot 0.5H_2O$ per batch (starting with 2 g Ca°). Because the solvents are fully evaporated during the rotary evaporation and oven-drying processes, no byproducts of the synthesis remain in the (phase pure) bassanite product (i.e., no further purification step is necessary).

To evaluate whether or not toluene was necessary for obtaining phase pure nanobassanite, a variation of this synthesis route involving the same steps above indicated, but without the addition of toluene was implemented.

**Characterization of precursor and product phases:**

Powders of precursor (Ca-ethoxide), product phases of the different runs performed, and the control (plaster of Paris, see below) were characterized using different analytical techniques. The mineralogy was determined by X-ray diffraction (XRD) on a PANalytical X'Pert Pro equipped with Ni filter (measurement parameters: Cu Kα radiation λ = 1.5405 Å, 45 kV, 40 mA, 3 to 70 °2θ exploration range, steps of 0.001 °2θ, and goniometer speed of 0.01 °2θ s$^{-1}$). Powder samples were deposited in zero-background Si sample holders for analysis. Mineral phases were identified by comparison with International Centre for Diffraction Data (ICDD) powder spectra and quantified by means of the Reference Intensity Ratio (RIR) method using the XPowder computer program.[S1] This computer program was also used to determine the Scherrer crystallite size of crystalline product phases.

Thermogravimetry coupled with differential scanning calorimetry (TG-DSC; Mettler-Toledo TGA/DSC1) was used to determine the amount of adsorbed and structural water in the product phase(s), as well as to identify the presence of residual (unreacted) precursor $Ca(OH)_2$ and possible carbonates (formed upon atmospheric $CO_2$ exposure during sample handling). TG was also used for the quantification of the synthesis yeild. DSC was used to identify α- and β-hemihydrate.[S2] For each run, the temperature was risen from 25 ºC up to 950 ºC at a heating rate of 20 K min$^{-1}$. In each measurement, ~40 mg sample mass was placed into an aluminium crucible, and weight loss and DSC data were continuously collected under either flowing air or $N_2$. No significant differences in the TG/DSC traces were observed between analyses performed in oxidizing and inert atmospheres, except for the run at 35'. In this latter case a very small exothermal band at 380-400 °C corresponding to the thermal oxidation of residual Ca-alkoxide was observed, which was absent in $N_2$ atmosphere, indicating that trace amounts of unreacted Ca-ethoxide were present in this run.

The shape, size, and ultrastructural features of precursor and product phases were studied using transmission electron microscopy (TEM) on a Titan and a Talos (FEI) with acceleration voltage of 300 kV and 200 kV, respectively. Prior to TEM observations, particles (powder samples) were dispersed in ethanol, sonicated for 30", and deposited on carbon-coated Cu grids. TEM observations were performed using a 40 µm objective aperture, which is a compromise between amplitude and phase contrast images. Selected area electron diffraction (SAED) images were collected using a 10 µm objective aperture. Such aperture allows collection of diffraction data from a circular area of ~0.2 µm diameter.

Solids were also analyzed by Fourier transform infrared spectroscopy using an attenuated total reflectance sample holder (ATR-FTIR, Jasco) in the spectral range 4000 – 400 cm$^{-1}$ with a step size of 0.48 cm$^{-1}$.

The particle size distribution (PSD) of products obtained at different reaction times was analyzed using dynamic light scattering (DLS), which yields the equivalent diameter of individual particles and aggregates. Solids were dispersed in ethanol, sonicated for 60", and measurements were conducted at a scattering angle of 180° using a Microtrac NANO-flex particle size analyzer equipped with a diode laser (λ = 780 nm, 5 mW) and a 1 m long flexible measuring probe (8 mm in diameter) with sapphire window as the sample interface. Scattering analysis was performed with an

acquisition time of 30 s during at least 10 consecutive measurements. PSDs were computed with the Microtrac FLEX application software package (v.11.1.0.2).

N$_2$ sorption isotherms of products obtained at different reaction times, as well as the control (plaster of Paris) sample, were obtained at 77 K on a Micromeritics TriStar 3000. Prior to measurement, powder samples (~250 mg sample mass) were heated at 80 °C for 4h and outgassed to 10$^{-3}$ Torr using a Micromeritics Flowprep. The BET analysis[S3] was used to determine the total specific surface area (SSA).

**Preparation of β-hemihydrate (plaster of Paris) control:**

The bassanite control was prepared by oven heating (under air atmosphere) commercially available gypsum (Sigma-Aldrich) at a temperature of 105 °C for 24 h. The bassanite obtained (pure phase β-hemihydrate) showed a specific surface area of 3.72 m$^2$/g, an average particle size of 1-2 μm (as determined using TEM), and a crystallite size (calculated using the Scherrer equation, using the most intense 200 Bragg reflection) of 49±2 nm. Note that the above indicated SSA for the obtained β-hemihydrate is standard for plaster of Paris.[S4]

**Measurement of the hydration kinetics:**

As indicated in the main text, two different experiments were performed in order to study the rate of hydration of the synthesized nanobassanite as compared to the control (plaster of Paris): (a) liquid-phase (LP) hydration through dissolution-reprecipitation, and (b) vapor-phase (VP) hydration through diffusion and condensation.[S5]

a) For the LP experiments, ~0.7/1 (wt/wt) water/bassanite mixtures of the nanobassanite (product obtained after 45' reaction time) and the control (standard β-hemihydrate, i.e., plaster of Paris) were prepared and immediately placed on zero-background silicon sample holders for XRD analysis. XRD patterns were collected continuously over an exploration range of 10-30 °2θ. Collection of each diffractogram took 7'. Successive XRD pattern were collected until complete bassanite to gypsum conversion was achieved. To quantify the degree of conversion, quantitative XRD analyses were performed using the RIR method. The fractional conversion, α was calculated using the following equation (Eq. (4)):

$$\alpha = \frac{100 - X_{bassanite}}{100} \qquad (4)$$

where $X_{bassanite}$ is the wt% of bassanite in the bassanite-gypsum mixture at each sampling time.

b) For the VP experiments, powdered nanobassanite (obtained after 35', 45' and 60' reaction time) and control (standard β-hemihydrate, i.e., plaster of Paris) samples were evenly spread on Petri dishes and placed inside a climatic chamber at a constant temperature of 22 °C and relative humidity of 90%. The

degree of conversion ($\alpha$) of bassanite into gypsum was monitored for one week and measured by means of XRD.

Considering that the $\alpha$ vs. time curves showed a sigmoid shape typical for Avrami-type kinetics, and the fact that previous studies have indicated that in fact the hydration kinetics of bassanite can be best described by an Avrami-type model,[S5] here we fitted our experimental data to the integral form ($g(\alpha)$) of the Avrami-Erofe'ev equation, which is widely used to describe solid state-transformations:[S6]

$$\alpha = 1 - exp[-k(t - t_0)^n]$$ (5)

where $n$ is a reaction exponent which provides information on the mechanism(s) of the reaction, $k$ is the rate constant (conversion rate), $t$ is the elapsed time, and $t_0$ is the induction time (extent of the induction period). Values of $t_0$ were determined by the intersection with the x-axis of the fitting line obtained by regression of the linear part of the $\alpha$ vs. $t$ plot for each hydration experiment. Eq. (5) is commonly considered to be valid for $0.15 < \alpha < 0.85$, but it has been used for higher (and lower) values of $\alpha$.[S7] Here it was used for $0.06 < \alpha < 0.99$.

A convenient way to rewrite Eq. (5) is the following:

$$\ln[-\ln(1 - \alpha)] = n \ln k + n \ln(t - t_0)$$ (6).

Plotting the left term in Eq. (6) vs. ln($t$-$t_0$) (the Sharp-Hancock plot) yields a linear graph if the Avrami-Erofe'ev model is valid for the system studied. A linear fit to such plotted experimental results will yield $n$ as the slope of the regression line and $k$ as the y-axis intercept.

The Avrami-Erofe'ev equation showed an overall good fitting ($R^2 \geq 0.97$) for all our experimental values (see main text). Obtained $n$ values were close to 1, which would mean that growth is one dimensional (1D) as has been previously observed for the kinetics of hemihydrate hydration.[S8] However, it is difficult to unambiguously determine the mechanism of reaction just based on $n$ values, as these values could indicate multiple possibilities.[S5] The $k$ values for liquid-phase hydration obtained here ($1.72 \cdot 10^{-3}$ to $2.56 \cdot 10^{-3}$ s$^{-1}$) are within the range of those previously reported for this reaction.[S5] As expected those obtained for vapor-phase hydration were (three) orders of magnitude lower (see main text).

**Cost estimate, potential applications and environmental impact:**

A rough estimate of the production costs of nanobassanite produced by the route described above was performed (Table S2). Considering its use in very specialized, high added-value applications concerning the conservation of invaluable cultural heritage objects as well as the production of biomaterials (i.e., bone grafting or design of regenerative material) and drug delivery systems, the costs seem justified and competitive. For instance, comparable nanomaterials used for the consolidation of heritage objects, such as commercial nanolimes (i.e., ethanol dispersions of $Ca(OH)_2$ nanoparticles), are currently sold for ~7-9 €/g of solid. The nanobassanite produced

here, which can be applied in an analogous way as nanolimes currently used for consolidation of the built heritage, has an estimated cost of 3.37 €/g of solid.

Regarding the environmental impact of the nanobassanite produced by the novel route described here, it should be taken into account that the synthesis procedure has a very high yield (≥ 99%), and that the environmental impact can be further minimized by recycling the solvents used during synthesis by fractional distillation, which would also reduce costs. It has to be acknowledged, however, that the production of metallic Ca used here for the synthesis of the alkoxide precursor requires an energy intensive processing (e.g., aluminothermic reduction of CaO at ~1200 °C). Nonetheless, the relatively small amounts of nanobassanite required for the high added-value uses proposed here, imply that the overall environmental impact of this novel synthesis route should be minimal.

## Supplementary references

S1. J. D. Martin-Ramos, *XPowder: A software package for powder X-Ray diffraction analysis*; http://www.xpowder.com, 2004.

S2. D. A. Powell, *Nature*, 1958, **182**, 792-792.

S3. K. S. W. Sing, D. H. Everett, R. A. W. Haul, L. Moscou, R. A. Pierotti, J. Rouquerol and T. Siemieniewska, *Pure Appl. Chem.*, 1985, **57**, 603-619.

S4. Y. B. Park, K. Mohan, A. Al-Sanousi, B. Almaghrabi, R. J. Genco, M. T. Swihart and R. Dziak, *Biomed. Mater.*, 2011, **6**, 055007.

S5. S. J. Gurgul, G. Seng and G. R. Williams, *J. Synchrotron Rad.*, 2019, **26**, 774-384

S6. M. Avrami, *J. Chem. Phys.*, 1940, **8**, 212-224.

S7. R. J. Hand, *Cem. Concr. Res.*, 1994, **24**, 885-895

S8. P. Mróz and M. Mucha, *Int. J. Eng. Res. Sci.*, 2017, **3**, 5-13.

**Supplementary Figures**
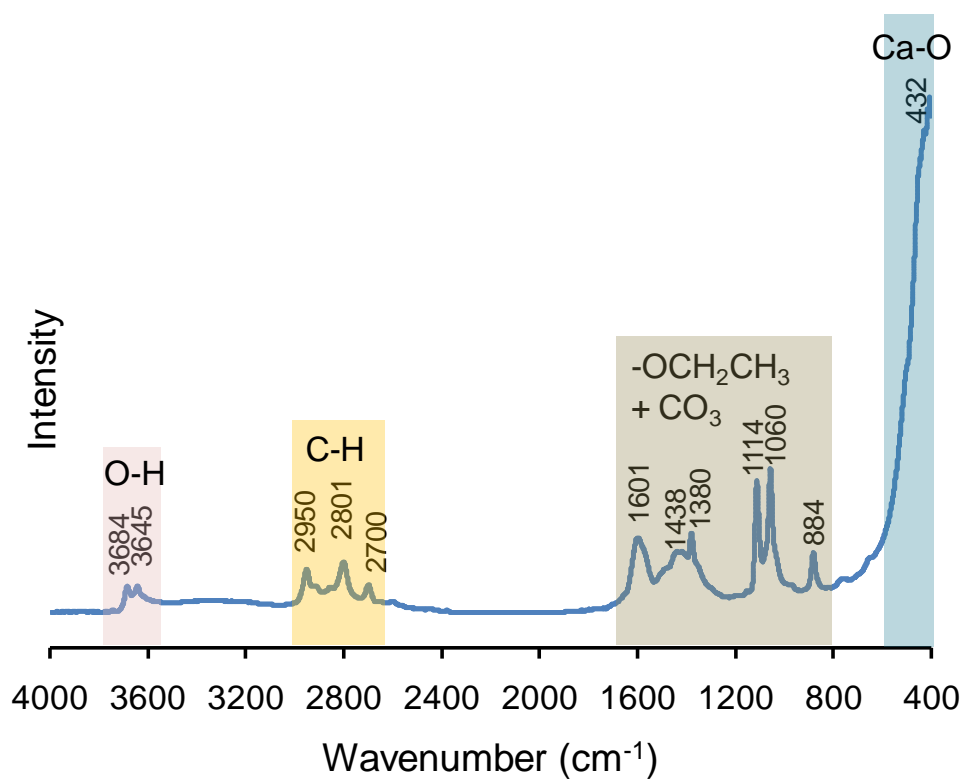


**Figure S1.** FTIR spectrum of precursor calcium ethoxide. The main IR bands are indicated.
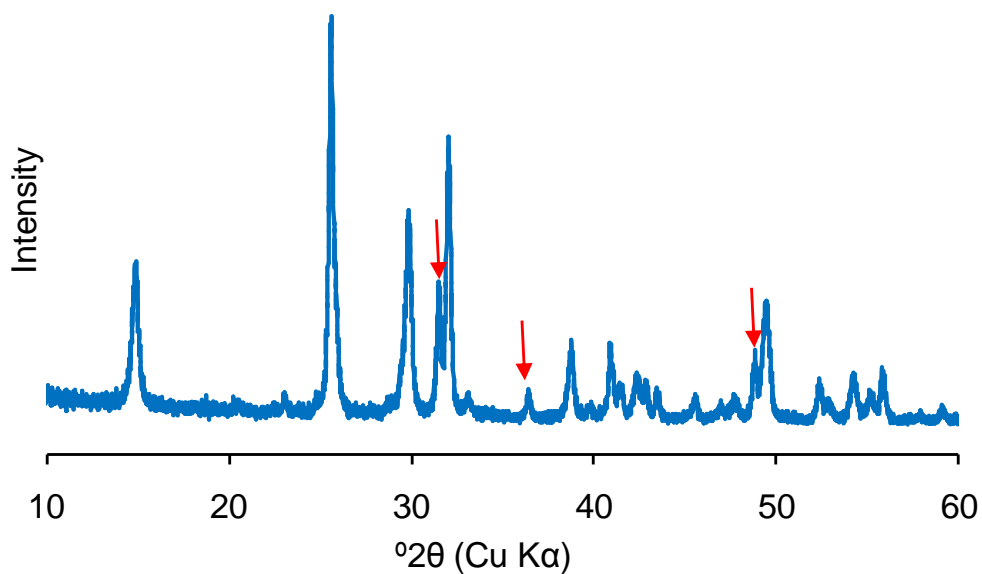
**Figure S2.** XRD pattern of the product obtained in the absence of toluene (60' reaction time). The 210, 022 and 230 Bragg peaks of soluble anhydrite at 31.46, 36.38 and 48.81 º2θ respectively (red arrows), are distinguishable from those of pure bassanite.
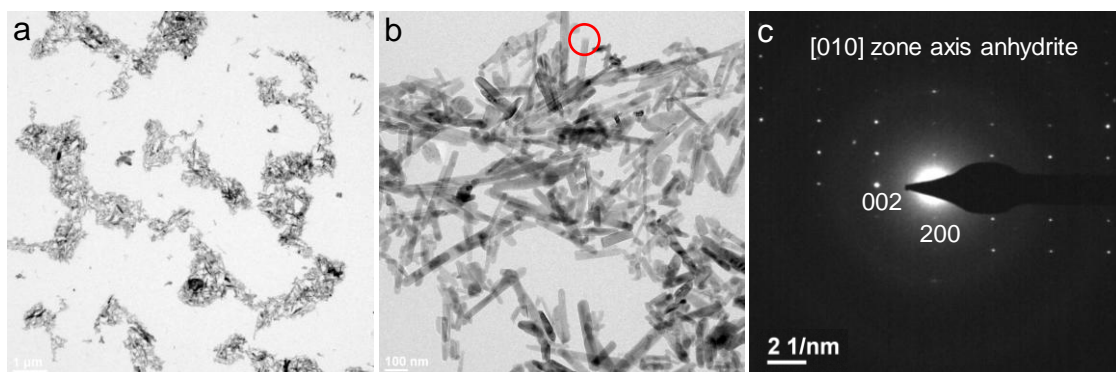


**Figure S3.** TEM images of the product obtained in the absence of toluene (35' reaction time). a) aggregates of a mixture of bassanite and anhydrite rod-shaped particles; b) detail of an aggregate of bassanite and anhydrite nanoparticles (they cannot be distinguished based on morphology); c) SAED pattern of the red-circled rod in (b) corresponding to [010] anhydrite zone axis.
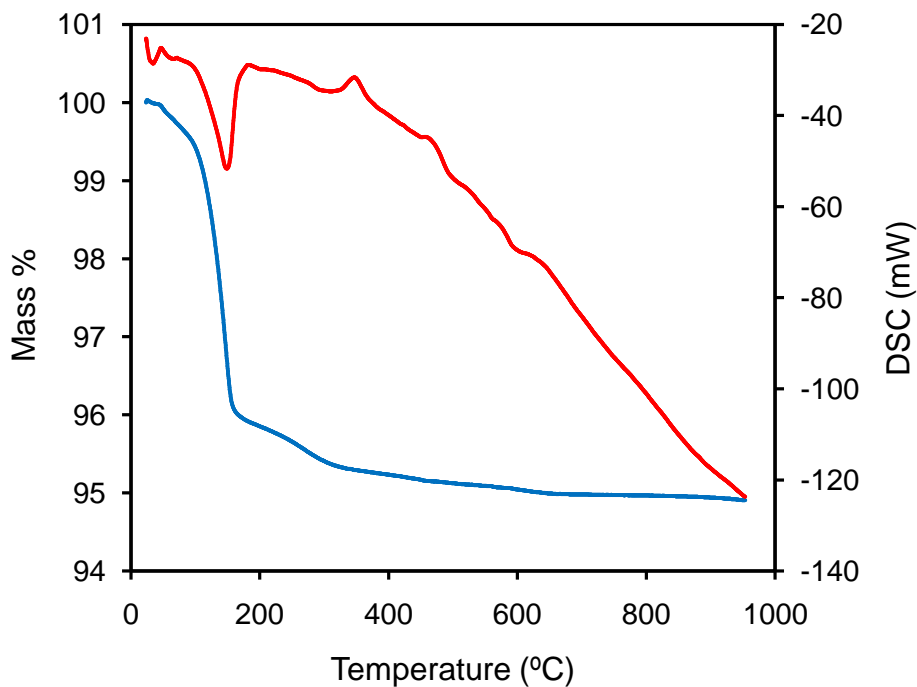
**Figure S4.** TG-DSC analysis of a sample prepared in the absence of toluene (60' reaction time). The DSC (red trace) allows the identification of bassanite as a synthesis product, however a mass loss of just ~4 wt% (after loss of adsorbed water at $T > 100$ °C) reveals that, in fact, this sample contains a significant fraction of anhydrite (i.e., the mass loss is inferior to the theoretical 6.2 wt% shown by bassanite when assuming a phase purity of 100%). The possible presence of gypsum was discarded, as only the endothermic peak of bassanite dehydration near 180 ºC was observed. These results are fully consistent with XRD results (see Fig. S2).

## Supplementary Tables

**Table S1.** Unit formula, XRD pattern codes (International Centre for Diffraction Data, ICDD) and structure codes (American Mineralogist Crystal Structure Database) of crystalline phases.

| Mineral | Unit Formula | Pattern Codes | Structure Codes |
|---|---|---|---|
| Anhydrite (soluble) | $CaSO_4$ | 01-086-2270 | 00019829 |
| Bassanite | $CaSO_4 \cdot 0.5H_2O$ | 00-041-0224 | 00019823 |
| Gypsum | $CaSO_4 \cdot 2H_2O$ | 01-074-1433 | 00020895 |
| Portlandite | $Ca(OH)_2$ | 01-081-2041 | 00009874 |

**Table S2.** Cost estimate of the production of nanobassanite according to the method reported here (excluding labor cost)

| Material | Standard Cost | Cost per gram |
|---|---|---|
| Ca, metallic (99%) | 52.60 €/100g | 0.15 € |
| Absolute ethanol | 14.24 €/L | 0.41 € |
| Toluene (anhydrous) | 48.30 €/L | 0.55 € |
| Sulfuric acid (95-98%) | 37.00 €/L | 0.02 € |
| Electric energy consumption | 0.17 €/kWh | 2.24 € (550 W heater / 24h) |
| Total | | 3.37 €/g (final product) |